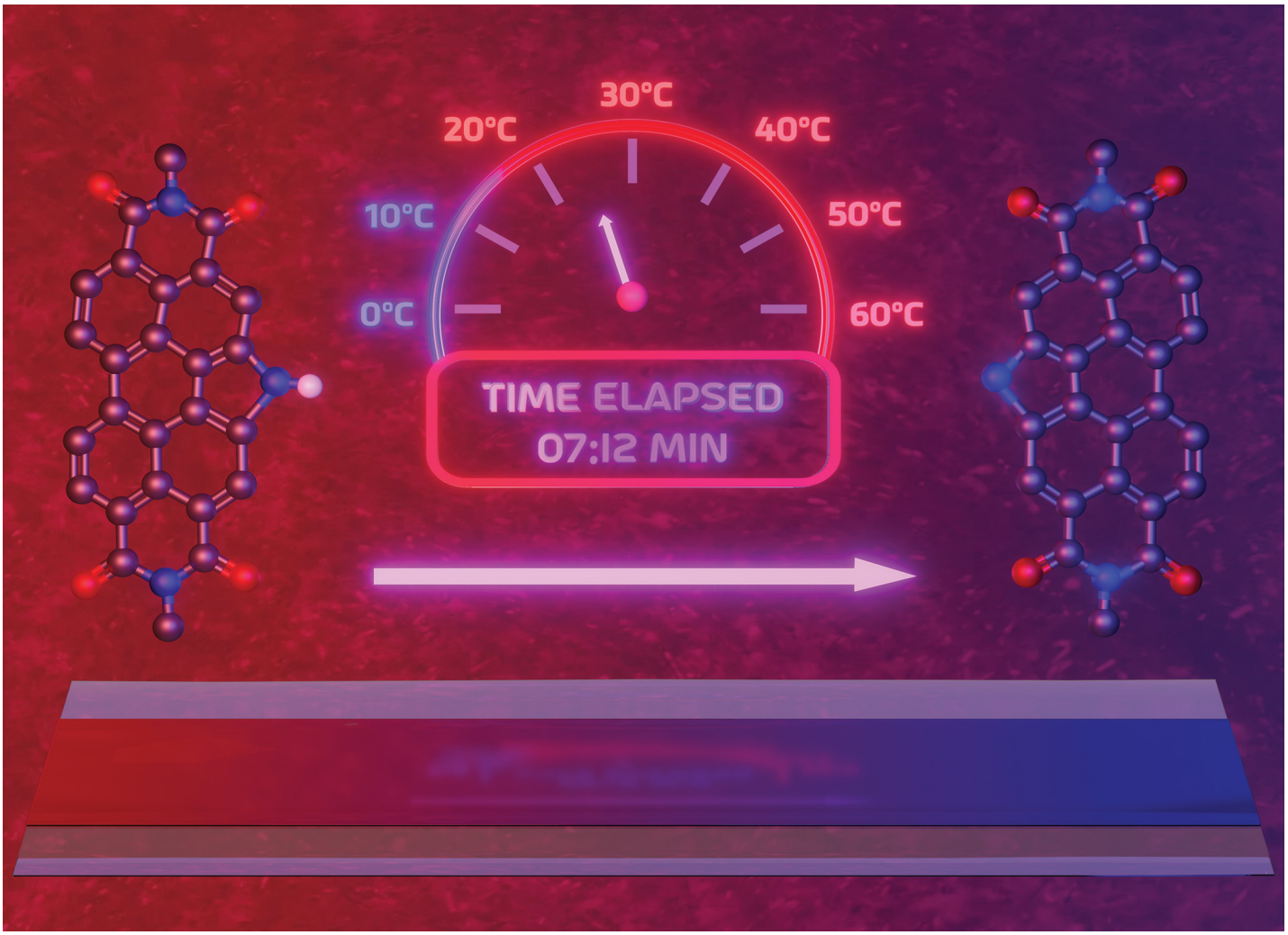

Showcasing research from Professor Welch's laboratory, Department of Chemistry, University of Calgary, Alberta, Canada. Cover image designed and illustrated by Kathryn M. Wolfe.

Tunable thermochromism in N-annulated perylene diimide thin films

Thermochromic films composed of N-annulated perylene diimide and poly(ethyleneimine) exhibit time-temperature dependent colour transitions. Thermal mixing activates acid-base chemistry, converting the neutral red chromophore into a deprotonated blue form to generate purple/indigo composite films.

Image reproduced by permission of Kathryn M. Wolfe from *Chem. Commun.*, 2026, **62**, 6319.

As featured in:

See Kathryn M. Wolfe and Gregory C. Welch, *Chem. Commun.*, 2026, **62**, 6319.

ROYAL SOCIETY OF CHEMISTRY

rsc.li/chemcomm

Registered charity number: 207890

ChemComm

COMMUNICATION

View Article Online
View Journal | View Issue

Cite this: *Chem. Commun.*, 2026, **62**, 6319

Received 5th December 2025,
Accepted 24th February 2026

DOI: 10.1039/d5cc06956d

rsc.li/chemcomm

Tunable thermochromism in N-annulated perylene diimide thin films

Kathryn M. Wolfe and Gregory C. Welch *

An N-annulated perylene diimide (PDIN-H) blended with branched polyethylenimine (PEI) and green solvents is coated to afford thermochromic thin films on a robust substrate. Tunable time-temperature colour transitions are observed with dependence on PDIN-H loading. UV-Visible spectra, chromaticity diagrams, (polarized) optical microscopy, and kinetic modelling reveal dynamic acid–base chemistry.

Thermochromic materials that undergo colour changes over time and at variable temperatures are experiencing emerging applications as time–temperature indicators (TTIs). When designed to be lightweight, low-cost, and robust, TTIs can be applied to packaging for increased product safety and efficiency in cold-chain logistics.[1–3] While inorganic and hybrid systems (*e.g.*, metal oxides, transition-metal complexes) deliver good stability,[4,5] organic chromophores, including natural dyes, are also targeted owing to facile optoelectronic tunability, lower cost, and green chemistry compatibility.[6] Among organic thermochromics, liquid crystals and leuco dyes are well-studied benchmarks. Thermotropic liquid crystals (nematic, smectic, and cholesteric phases) can show vivid, reversible colour shifts over defined temperature ranges and have been used in thermal mapping,[7] displays,[8,9] and medical/industrial sensors.[10] The drawbacks to these systems can include limited mechanical robustness, sensitivity to UV or environmental degradation, and sometimes complex alignment or encapsulation requirements. Leuco dyes can change chemical structure with heat, an example being spiropyrans.[11,12] While organic thermochromism is common, a challenge is to develop functional systems for applied temperature monitoring. Recent examples of novel, applied organic thermochromic systems include (1) an ultrathin polymer blend composed of organic (poly(ethylene oxide)) and inorganic components (poly(dimethyl siloxane)) that showcase tunable thermochromic temperature ranges and high durability for smart coatings,[13] (2) thermochromic liquid crystalline elastomers combining mechanical flexibility and vivid colour transitions,[14] and (3) smart surfaces using cholesteric LCs on leather or flexible substrates to yield thermally reversible colour effects.[15] Our previous work demonstrated that N-annulated perylene diimide (PDIN-H) in thin film form deprotonates in the presence of volatile amines, undergoing a clear, visible colour change (from the PDIN-H neutral state to the ionic deprotonated state, $PDIN^-$; Fig. 1a).[16–18] In this work, we extend this concept by fabricating green solvent processed thermochromic thin films on a robust substrate, thus demonstrating practical use. Here, the use of branched polyethyleneimine (PEI, Fig. 1b) provides a non-volatile biopolymer equipped with Lewis basic sites for facilitating reversible acid–base mechanisms dependent on temperature. We tracked thermochromic behaviour *via* UV-visible spectroscopy, digital photography (chromaticity), and optical microscopy to

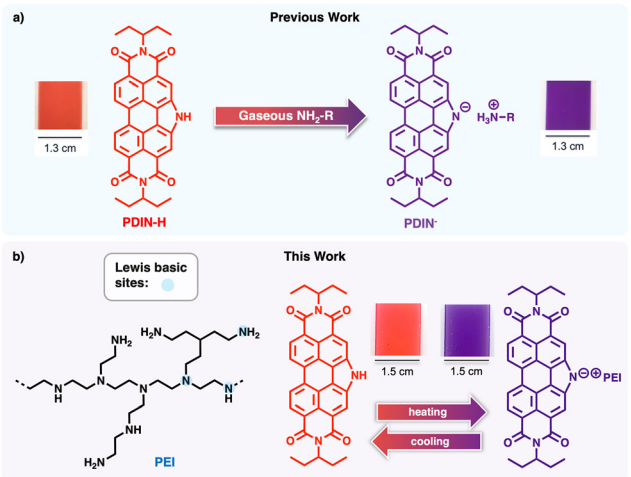

Fig. 1 Acid–base dependent colour changes for PDIN-H; (a) previous work highlights that PDIN-H thin films act as colorimetric gaseous amine indicators, turning from red to purple upon volatile amine exposure,[16] and (b) this work utilizes the established acid–base chemistry by introducing the non-volatile biopolymer, PEI, decorated with Lewis basic amino groups allowing for reversible thermochromic behaviour in film form.

Department of Chemistry, University of Calgary, 2500 University Drive N.W., Calgary, Alberta, Canada T2N 1N4. E-mail: gregory.welch@ucalgary.ca

demonstrate a flexible, scalable TTI candidate with high optical contrast.

Solution UV-visible spectra for neutral and deprotonated PDIN-H are provided in the SI (Fig. S1). In tetrahydrofuran (THF), neutral PDIN-H shows a sharp absorption maximum at 521 nm (red solution). In the strong organic base 1,8-diazabicyclo[5.4.0]undec-7-ene (DBU), the spectrum is red-shifted but retains a vibronic structure, with a new λ_{max} at 620 nm characteristic of the anionic form, $PDIN^-$ (blue solution). These spectral signatures are consistent with previous reports of PDIN-H deprotonation.[16,17,19–21] Solution thermochromism was also probed: in neat butylamine at 30 °C, PDIN-H exists as a mixture of PDIN-H and $PDIN^-$, but heating to 100 °C largely restores the neutral PDIN-H spectrum (Fig. S2). In a 1 : 1 butylamine/water mixture (Fig. S3), a high fraction of $PDIN^-$ is present at 30 °C with a small fraction reverting to PDIN-H at 100 °C. We attribute the reduced reversibility in the BA/water mixture to hydroxide formation (pK_a of BA = 10.6),[22] which increases the effective basicity of the medium and thus favours deprotonation even upon heating.

To translate the acid–base colorimetric behaviour into thin film form, we formulated green solvent based inks for coating organic chromophores onto plastic substrates. As previously shown, ethyl lactate and 2-methyltetrahydrofuran can be blended with amines to afford concentrated PDIN-H-based inks suitable for coating.[19] Polycarbonate was chosen as the substrate owing to high optical quality. As shown in Fig. S4, inks of PDIN-H, PEI, and a PDIN-H/PEI composite were individually slot-die coated onto the plastic substrates (see the SI for full methodology). Films from PDIN-H-only inks appear red (Fig. S4b), whereas PEI-only films are transparent (Fig. S4d). PDIN-H/PEI composite inks yield indigo films, and this colour persists after annealing/drying (Fig. S4f and Fig. 2a). We previously showed that PDIN-H inks containing volatile primary amines, such as butylamine, gave wet purple films that dry red, indicating PDIN-H deprotonation in the ink followed by re-protonation as the amine evaporates.[16] In contrast, PEI is a non-volatile, highly viscous liquid that remains in the film after coating. In the PDIN-H/PEI composite films, the primary, secondary and tertiary amines in PEI deprotonate PDIN-H, giving a mixture of red PDIN-H and blue $PDIN^-$ and thus a purple/indigo appearance. Film UV-visible spectra support this assignment: PDIN-H-only films display a neutral PDI spectrum, PEI-only films are featureless, and the PDIN-H/PEI composite shows contributions from both PDIN-H and $PDIN^-$. The PDIN-H and PEI films were probed for uniformity *via* optical microscopy (OM) and polarized optical microscopy (POM), with both films displaying a high degree of uniformity (Fig. S5).

Next, we examined thin film thermochromic behaviour. Inks containing dispersed PDIN-H (5 mg mL^{-1}) and PEI (200 mg mL^{-1}) were slot-die coated onto polycarbonate substrates and annealed at 100 °C for 15 min, giving indigo films that turned red upon cooling to 0 °C (Fig. 2a and Fig. S6a). On warming back to room temperature (20 °C; Fig. 2d), the films changed from red (neutral PDIN-H) to purple (mixed PDIN-H/$PDIN^-$) and then to indigo (predominantly $PDIN^-$). These colour changes were

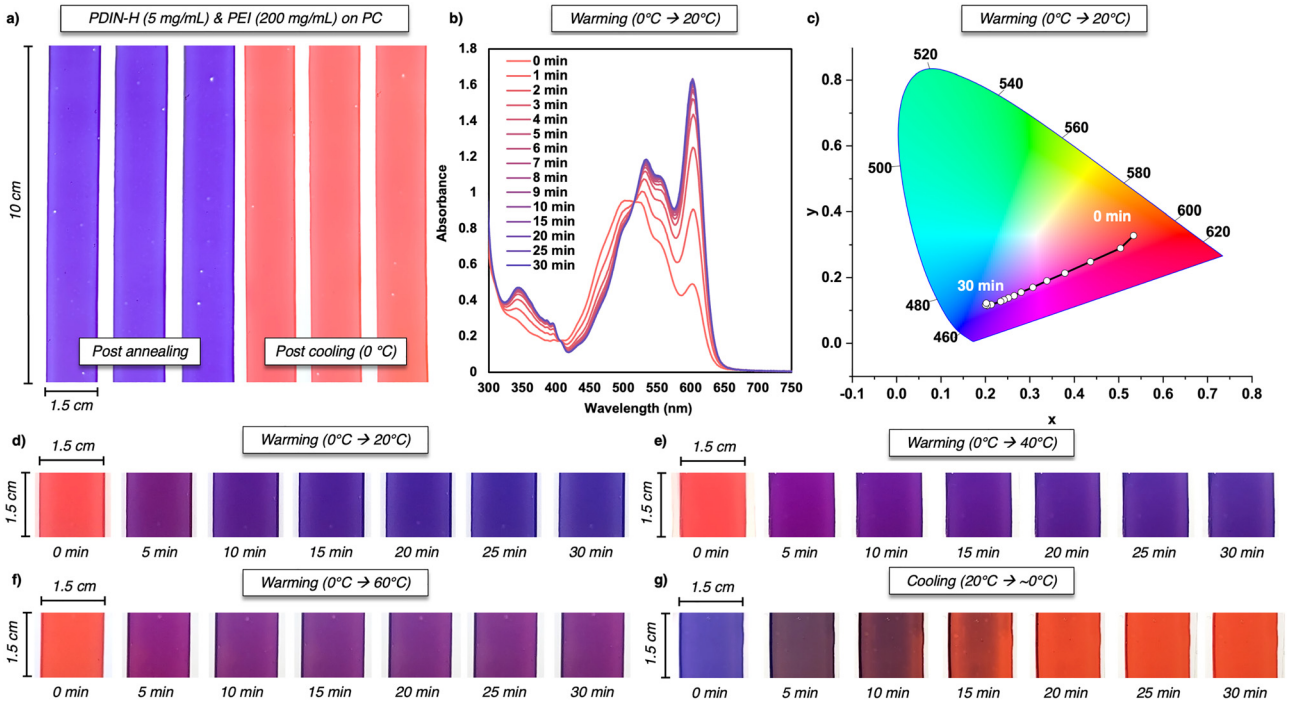

Fig. 2 Time-temperature profiling of PDIN-H/PEI composites as thin films on polycarbonate: (a) digital photographs of the films post-coating/annealing at 100 °C for 15 minutes and post-cooling to 0 °C, (b) UV-visible spectra of time-resolved colour changes upon warming a film from 0 °C to 20 °C, (c) chromaticity diagram of a film upon warming from 0 °C to 20 °C, and digital photographs of the films at variable time intervals when (d) warmed from 0 °C to 20 °C, (e) warmed from 0 °C to 40 °C, (f) warmed from 0 °C to 60 °C, and (g) cooled from 20 °C to 0 °C (post cool–warm cycle). See Fig. S7 (SI) for additional photographs.

monitored by digital photography (Fig. 2a, d–g and Fig. S6a, S7), UV-visible spectroscopy (Fig. 2b and Fig. S6b), and chromaticity diagrams/data (Fig. 2c and Fig. S8 and Tables S1–S4). The UV-visible spectrum at $t = 0$ min shows broadened peaks characteristic of aggregated PDIN-H.[21] Upon warming to 20 °C, two isosbestic points at 407 nm and 515 nm and growth of the 602 nm band indicate an A → B process ([PDIN-H] + [PEI] → [$PDIN^-$ + PEI^+]). The sharp 602 nm peak is consistent with a non-aggregated $PDIN^-$ state, suggesting good intercalation of $PDIN^-$ and PEI^+. We also evaluated film stability *via* thermal stressing (Fig. S9) and thermal cycling (Fig. S10), demonstrating high thermal robustness and reproducible cycling; however, we did observe decreased thermochromic performance after prolonged storage (~1 month at 0 °C in the dark), which we attribute to the oxidation of PEI.[23,24] For cold-chain TTI applications, the response at different exposure temperatures is critical to model.[25] Therefore in addition to warming to 20 °C, we warmed the PDIN-H/PEI composite films to 40 and 60 °C (using a hot plate) and quantified the colour changes using digital photography and chromaticity diagrams (Fig. 2d–f and Fig. S8a–c and Tables S1–S3). When warmed to 20 °C, the films are indigo with a high blue component at $t = 30$ min ($B = 159$; Table S1). When warming to 40 °C and 60 °C, blue character was reduced to $B = 154$ (Table S2) and $B = 130$ (Table S3) at $t = 30$ min, respectively. Therefore, higher temperatures lead to a lower degree of PDIN-H deprotonation. We attribute this to two effects: (1) amine basicity decreases with temperature,[26] and (2) increased thermal motion disrupts the ionic pairs. Importantly, the PDIN-H/PEI films remain reversible: after warming from 0 to 20 °C, placing the films on an ice pack returns the colour to red (Fig. 2g). Note, the colour trajectory upon cooling bypasses the purple state, turning brown before returning to red.

OM and POM were used to visualize morphological changes upon warming (Fig. 3). After coating (Fig. 3a), the indigo films have defined domains uniformly dispersed. Upon cooling to 0 °C (Fig. 3b), small bright spots emerge in both the OM and POM images, which we attribute to domains of aggregated PDIN-H, consistent with the UV-visible spectra in Fig. 2b. Warming to 20 °C for 5 min causes the bright spots to disappear and new, darker domains form (Fig. 3c), which diminish after ~10 min at 20 °C (Fig. 3d). The data suggest the following: (1) post-coating/annealing, the composite is well mixed and contains a high fraction of $PDIN^-/PEI^+$, (2) cooling to 0 °C promotes phase separation of PDIN-H and PEI, yielding aggregated PDIN-H domains, (3) warming from 0 °C remixes PDIN-H and PEI, regenerating $PDIN^-/PEI^+$, and (4) higher warming temperatures reduce the extent of deprotonation due to increased molecular motion and lower amine basicity in PEI.

To probe the tunability of the PDIN-H/PEI reaction rate at 20 °C, we prepared composite films by increasing PDIN-H loading (5, 10 and 15 mg mL^{-1}) with a fixed PEI load (200 mg mL^{-1}) (Fig. 4 and Fig. S11, S12). These inks were prepared by shaking, instead of sonication, as prolonged sonication caused visible phase separation. While 5 mg mL^{-1} PDIN-H can be fully dispersed by mild sonication, higher loadings were not fully miscible even with extended sonication. Additionally, solvent engineering by incorporation of butylamine for full dissolution was attempted, but

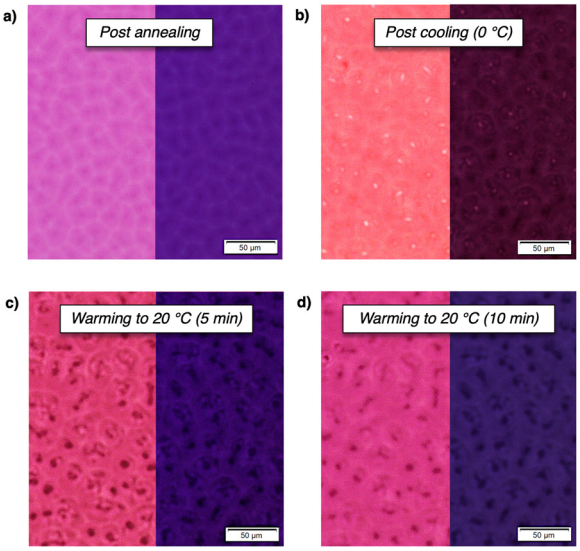

Fig. 3 Optical and polarized optical microscopy images of **TTI-5S** films: (a) post-annealing at 100 °C for 15 min, (b) post-cooling to 0 °C, (c) warming from 0 °C to 20 °C after 5 minutes, and (d) warming from 0 °C to 20 °C after 10 minutes.

reduced thermochromism in the thin films (see the SI for ink engineering methods). For clarity, we denote the film made with sonicated 5 mg mL^{-1} PDIN-H/200 mg mL^{-1} PEI ink as **TTI-5S** (Fig. 2 and Fig. S6, S7), and the films made from the shaken inks with 5, 10 and 15 mg mL^{-1} PDIN-H loading as **TTI-5**, **TTI-10** and **TTI-15**, respectively (Fig. 4 and Fig. S11, S12). All shaken inks were slot-die coated onto polycarbonate substrates, yielding uniform thin films (Fig. S11), albeit PDIN-H crystallites are present as seen in OM/POM (Fig. S13–S15). The higher the loading of PDIN-H, the higher the degree of crystallites present. UV-visible spectra collected immediately after coating and after overnight drying at 0 °C show higher absorbance for **TTI-10** and **TTI-15**, with similar spectral shapes (Fig. S11e and f). All as-coated films exhibit sharp vibronic features consistent with non-aggregated PDIN-H, whereas cooling/drying at 0 °C induced aggregation (Fig. S11d–f). On warming from 0 to 20 °C, optical changes monitored by UV-visible spectroscopy and digital photography (Fig. 4) revealed faster acid–base reactivity at lower PDIN-H loading: changes plateau at ~30 min for **TTI-5**, ~45 min for **TTI-10**, and ~90 min for **TTI-15** (Fig. S12). Consistent with this, chromaticity data (Fig. S16 and Tables S5–S7) reveal that **TTI-5** reaches a blue-rich colour at 90 min ($B = 151$), while **TTI-10** ($B = 99$) and **TTI-15** ($B = 82$) have less blue character at 90 min. Chromaticity diagrams show a time-dependent colour evolution: **TTI-5** has the largest shift within the first 10 minutes, whereas **TTI-10** and **TTI-15** exhibit larger shifts after 10 minutes.

Kinetic modelling of TTIs is common;[25,27,28] here, we used UV-visible spectra to model our system as a pseudo-first-order reaction with respect to PDIN-H, as PEI is in excess (see the SI for details; Fig. S17–S19). Four important aspects: (1) PDIN-H is aggregated at 0 °C and mixes with PEI upon warming, (2) an initial period of thermal equilibration occurs upon warming, (3) once mixed, PDIN-H converts to $PDIN^-$ with no detectable by-products,

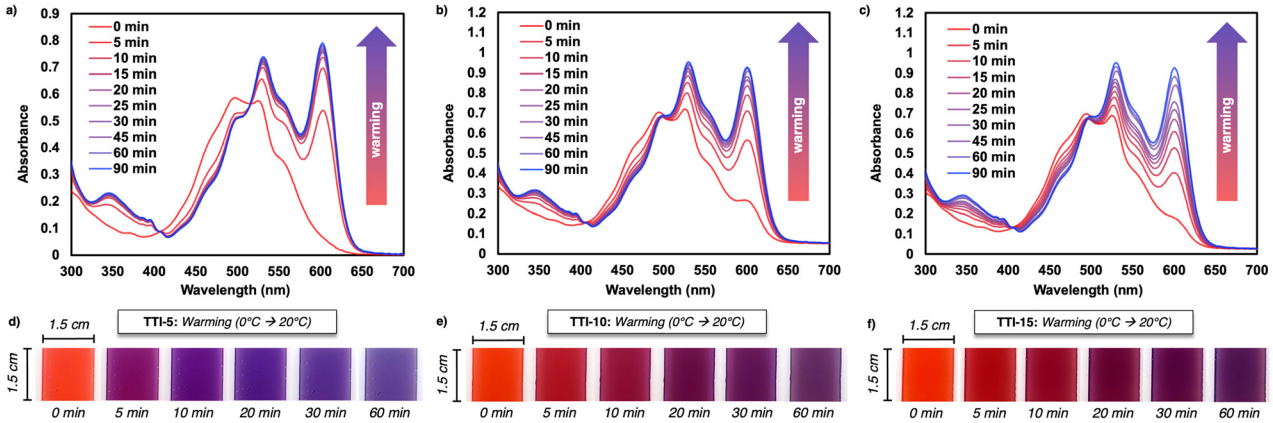

Fig. 4 Time-temperature profiling of **TTI-5**, **TTI-10**, and **TTI-15** films: UV-visible spectra of time-resolved colour changes upon warming (a) a **TTI-5** film, (b) a **TTI-10** film, and (c) a **TTI-15** film from 0 °C to 20 °C, and digital photographs of (d) **TTI-5**, (e) **TTI-10**, and (f) **TTI-15** films when warmed from 0 °C to 20 °C over time. Film widths are 1.5 cm. See Fig. S12 for additional photographs.

as supported by isosbestic points in the UV-visible spectra, and (4) PEI being a viscous liquid within the probed temperature range enables the mixing dynamics. The resulting apparent rate constants (k') are 0.579 min^{-1} (**TTI-5S**), 0.092 min^{-1} (**TTI-5**), 0.063 min^{-1} (**TTI-10**), and 0.033 min^{-1} (**TTI-15**). Overall, increasing the PDIN-H content slows the kinetics, which we attribute to an equilibrium shift toward neutral PDIN-H (Le Châtelier's principle), although we recognize further studies are needed.

In summary, we demonstrate a green route to PDIN-H/PEI composite thin films as proof-of-concept TTIs with a tunable response. Reversible PDIN-H/PEI acid–base chemistry yields pronounced, reversible colour changes from 0 to 60 °C (red neutral to blue deprotonated), readily tracked optically. UV-visible spectroscopy, OM/POM, and kinetic analyses indicate that PDIN-H loading controls the rate and extent of composite deprotonation, thus highlighting a facile method for tuning TTI response. However, PEI's susceptibility to oxidation motivates either replacing PEI with alternative polymer matrices bearing basic moieties to improve stability and reproducibility, or pursuit of encapsulation with more in-depth studies on reactivity. Overall, the use of PDIN-H for TTIs is intended to inspire scalable, sustainable indicators, with clear paths for material optimization and electronic integration given PDIN-H's role as an electron-transport material.

Author contributions

K. M. W. performed all experiments and wrote the manuscript while G. C. W. guided experiments and edited the manuscript.

Conflicts of interest

The authors have no conflicts to declare.

Data availability

Supplementary information (SI) is provided electronically. Supplementary information is available. See DOI: https://doi.org/10.1039/d5cc06956d.

Acknowledgements

The authors warmly thank Muhammad Rizwan Khan Niazi, Mary Odagwe, and Rebecca Ginesi for all the work they did that enabled this discovery. This project was supported by the NSERC Discovery Grant program (RGPIN-2025-04443) and the NSERC Strategic Network Green (NETGP 508526-17). KMW is grateful for the scholarships that enabled this work, and thanks NSERC and Alberta Innovates.

References

1 M. S. Yar, I. Henry Ibeogu, M. Adnan, F. Rehman, A. Regmi, M. Zhou, M. Bilal, Z. Liu, H. K. Bako and C. Li, *Food Chem.*, 2025, **480**, 143906.
2 L. T. Hao, M. Lee, H. Jeon, J. M. Koo, S. Y. Hwang, D. X. Oh and J. Park, *ACS Omega*, 2021, **6**, 8598–8604.
3 N. D'Uva, F. Camera, S. Amendola, S. Nappi, C. Miozzi, C. Occhiuzzi and G. Marrocco, *2021 IEEE International Workshop on Metrology for Industry 4.0 & IoT (MetroInd4.0&IoT)*, IEEE, Rome, Italy, 2021, pp. 145–149.
4 M. Wan, H.-R. Chen, Y.-N. Wang, K. Shi, J.-Y. Liu, Z.-M. Li, S.-Y. Ye, J.-Y. Li and L.-Z. Chen, *Mater. Chem. Front.*, 2022, **6**, 3094–3101.
5 J. Jin, J. Zhang, J. Zhang, X. Chen, S. Zou, Y. Xin, S. Liu, G. Liu, X. Yan and J. Huang, *Adv. Mater.*, 2025, **37**, 2416146.
6 P. H. N. Crosby and A. N. Netravali, *Adv. Sustainable Syst.*, 2022, **6**, 2200208.
7 V. Miskovic, E. Malafronte, C. Minetti, H. Machrafi, C. Varon and C. S. Iorio, *Front. Bioeng. Biotechnol.*, 2022, **10**, 806362.
8 Y.-L. Li, N.-N. Li, D. Wang, F. Chu, S.-D. Lee, Y.-W. Zheng and Q.-H. Wang, *Light: Sci. Appl.*, 2022, **11**, 188.
9 H. Wang, H. K. Bisoyi, L. Wang, A. M. Urbas, T. J. Bunning and Q. Li, *Angew. Chem., Int. Ed.*, 2018, **57**, 1627–1631.
10 W. Iglesias, N. L. Abbott, E. K. Mann and A. Jákli, *ACS Appl. Mater. Interfaces*, 2012, **4**, 6884–6890.
11 M. Jamali, A. R. Sardarian, F. Rezaei, A. Mohajeri, M. M. Ghanbari and G. Batta, *Sci. Rep.*, 2025, **15**, 20570.
12 M. A. Gerkman, S. Yuan, P. Duan, J. Taufan, K. Schmidt-Rohr and G. G. D. Han, *Chem. Commun.*, 2019, **55**, 5813–5816.
13 S. K. Saju, A. B. Puthirath, S. Wang, T. Tsafack, L. K. Beagle, A. Baydin, N. Chakingal, N. Komatsu, F. Tay, A. Sharma, R. Sreenivasan, J. Kono, R. Vajtai, N. R. Glavin, Y. Long and P. M. Ajayan, *Joule*, 2024, **8**, 2696–2714.
14 C.-Y. Kuo, Y.-T. Lin, T.-T. Huang and C.-Y. Liu, *ACS Appl. Polym. Mater.*, 2024, **6**, 9080–9087.
15 C.-A. Alexe, C. Gaidau, I. R. Stanculescu, C. Burducea and V. Cîrcu, *J. Nat. Fibers*, 2025, **22**, 2519618.

16 C. R. Harding, J. Cann, A. Laventure, M. Sadeghianlemraski, M. Abd-Ellah, K. R. Rao, B. S. Gelfand, H. Aziz, L. Kaake, C. Risko and G. C. Welch, *Mater. Horiz.*, 2020, **7**, 2959–2969.
17 M. J. Grant, A. Hoff, L. G. Kaake and G. C. Welch, *Sens. Diagn.*, 2024, **3**, 817–821.
18 M. Courté, A. Hoff, G. C. Welch and L. G. Kaake, *J. Mater. Chem. C*, 2024, **12**, 5083–5087.
19 K. M. Wolfe, Z. T. Gardner, Z. M. Smith, A. Harrison, C. Risko and G. C. Welch, *Chem. Sci.*, 2025, DOI: 10.1039/D5SC06640A.
20 M. Vespa, J. R. Cann, S. V. Dayneko, O. A. Melville, A. D. Hendsbee, Y. Zou, B. H. Lessard and G. C. Welch, *Eur. J. Org. Chem.*, 2018, 4592–4599.
21 M. E. Farahat, M. A. Anderson, M. Martell, E. L. Ratcliff and G. C. Welch, *ACS Appl. Mater. Interfaces*, 2022, **14**, 43558–43567.
22 F. M. Jones and E. M. Arnett, in *Progress in Physical Organic Chemistry*, ed. A. Streitwieser and R. W. Taft, Wiley, 1st edn, 1974, vol. 11, pp. 263–322.
23 C. Yan and A. Sayari, *Chem. Eng. J.*, 2024, **479**, 147498.
24 W. Buijs, *Nanomaterials*, 2025, **15**, 313.
25 A. T. Pandian, S. Chaturvedi and S. Chakraborty, *Food Measure*, 2021, **15**, 1523–1540.
26 M. Gupta, E. F. Da Silva and H. F. Svendsen, *J. Phys. Chem. B*, 2012, **116**, 1865–1875.
27 B. Ye, J. Chen, H. Ye, Y. Zhang, Q. Yang, H. Yu, L. Fu and Y. Wang, *Food Chem.*, 2022, **373**, 131448.
28 Y. Galagan, S.-H. Hsu and W.-F. Su, *Sens. Actuators, B*, 2010, **144**, 49–55.